Available online at www.sciencedirect.com
SCIENCE DIRECT®
Continental Shelf Research 24 (2004) 337–351
CONTINENTAL SHELF RESEARCH
www.elsevier.com/locate/csr

Incremental inference of boundary forcing for a three-dimensional tidal model: tides in the Taiwan Strait

Sen Jan[a,*], Yu-Huai Wang[b,1], Dong-Ping Wang[c], Shenn-Yu Chao[d]

[a] *Institute of Physical Oceanography, National Sun Yat-Sen University, Kaohsiung 80424, Taiwan, ROC*
[b] *National Center for Ocean Research, P.O. Box 23-13, Taipei 10617, Taiwan, ROC*
[c] *Marine Science Research Center, State University of New York, Stony Brook, NY 11794-5000, USA*
[d] *Horn Point Laboratory, University of Maryland Center for Environmental Science, P.O. Box 0775, Cambridge, MD 21613-0775, USA*

Received in revised form 12 December 2002; accepted 17 November 2003

Abstract

Tides in the Taiwan Strait are predominantly semidiurnal. The semidiurnal tide propagates southward along the mainland (China) coast but is a standing wave on the Taiwan coast. The tidal amplitude is large, reaching about 2 m in the middle of the strait, but diminishing rapidly towards the deeper portion of the strait. An amphidromic point is located off the southwest coast of Taiwan. Tidal currents are strong near the open ends (especially on the Taiwan side) and diminish towards the middles of the strait. A fine-resolution (3 km × 3 km), three-dimensional, coastal ocean model is being developed for the Taiwan Strait. In this study, the focus is on validation of tidal sea levels and currents. The limited-area model is driven by tidal elevations on two open ends, of which amplitudes and phases are optimized through a four-dimensional variational assimilation. Specifically, the model uses an incremental approach in which misfits between model results and coastal tidal observations are reduced incrementally through repeat applications of a linear two-dimensional model and its adjoint. The incremental approach is both effective and efficient. The root-mean-squared (rms) error for the dominant M_2 tide is reduced from about 0.15 to 0.06 m, a five-fold reduction in error variance. Moreover, this is achieved with only 3–4 iterations of the three-dimensional model; for comparison, a typical four-dimensional variational assimilation will require an order of magnitude more computation effort. The predicted tidal current ellipses are also compared with the observations from six bottom-mounted Acoustic Doppler Current Profilers (ADCP). The semi-major axis currents generally agree to within 0.05 m/s. The sensitivity of vertical tidal current structure to bottom friction also is examined.

Keywords: Tides; Taiwan Strait; Four-dimensional variational assimilation; Adjoint

1. Introduction

Sophisticated three-dimensional ocean general circulation models are now used routinely in coastal ocean forecast/nowcast systems. In Taiwan, the National Center for Ocean Research (NCOR) has undertaken a major effort to develop

*Corresponding author. Now at: Institute of Hydrological Sciences, National Central University, Jung-li 320, Taiwan, ROC. Tel.: +886-3-422-3410; fax: +886-3-422-2894.
E-mail address: senjan@cc.ncu.edu.tw (S. Jan).
[1] Now at: Institute of Physical Oceanography, National Sun Yat-Sen University, Kaohsiung 804, Taiwan, ROC.

0278-4343/$ - see front matter © 2003 Elsevier Ltd. All rights reserved.
doi:10.1016/j.csr.2003.11.005

a fine-resolution Taiwan Strait Nowcast System (TSNOW) with goals of making timely predictions of sea levels (storm surges), ocean currents, and frontal locations. Such operational nowcast system can be used for disaster mitigation, rescue and search, environment policy making, fishery, and marine resources management. The plan for TSNOW is to include both tidal and mean currents. Tidal motion accounts for a significant portion of the sea level and current variability in the Taiwan Strait; spectral analysis consistently suggested that most pronounced peaks are at tidal frequencies (Chuang, 1985). During the first stage of the model development, our goal is to produce accurate barotropic tidal predictions.

The Taiwan Strait, about 400 km long and 200 km wide, is a passage connecting the East and South China Seas (Fig. 1). While its main water body is relatively shallow (~60 m) and flat, the strait connects to the South China Sea through a series of complex topographic features, including the shallow Taiwan Banks on the southwest end and the steep-sided deep Penghu Channel on the southeast end of the strait. There have been several tidal model studies for the Taiwan Strait with various complexities. The most recent tidal models include Lin et al. (2000) with a mild-slope finite-element model and Jan et al. (2002) with a finite-difference primitive-equation model. In both studies, the model encloses part of the East China

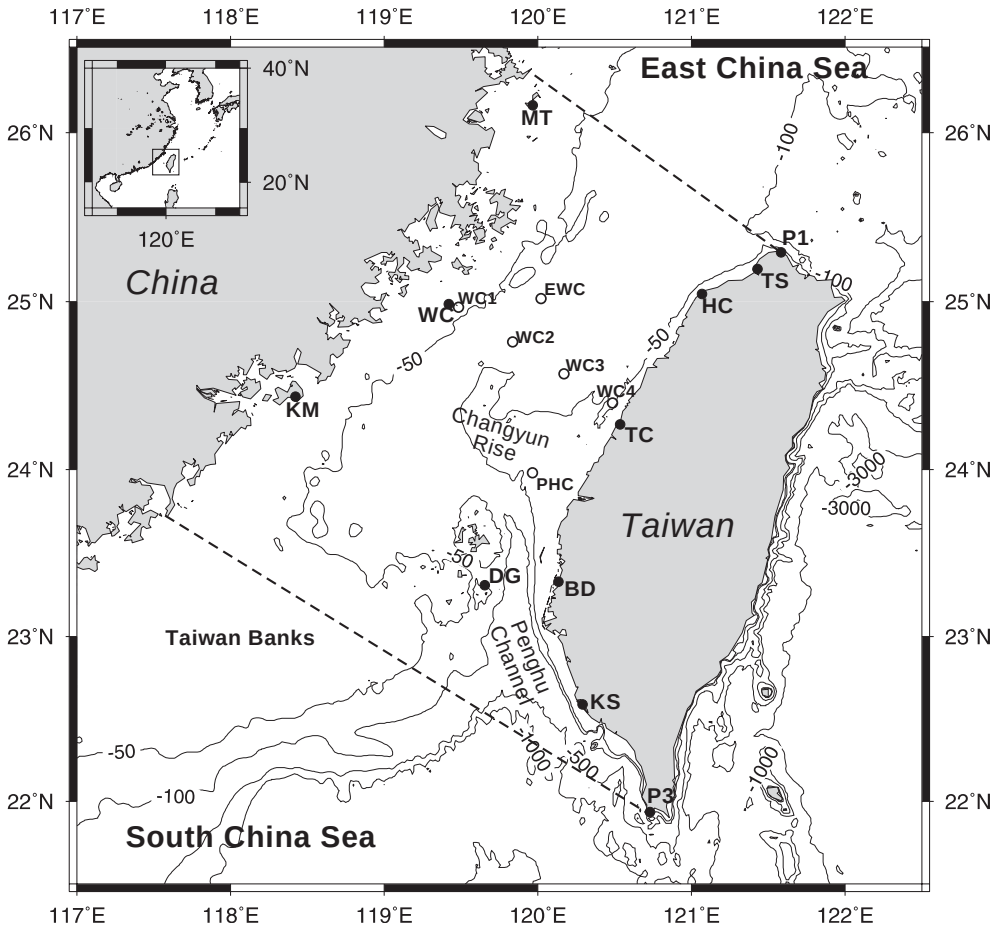

Fig. 1. The Taiwan Strait Bathymetry. The full circles represent the tide-gage stations, the open circles the bottom-mounted ADCP moorings, and the dashed lines the model's open boundary.

Sea and South China Sea, and the tidal forcing (tidal amplitude and phase) is prescribed on an open boundary far east of Taiwan. In Lin et al. (2000) the incident wave amplitude is adjusted for the best fit, and in Jan et al. (2002) the open ocean tides are derived from the global tidal model results of Kantha (1995). Both models produce results comparable to the state-of-the-art. For example, the average amplitude difference between observed and predicted M_2 tides in Lin et al. (2000) is 0.14 m. This result compares favorably with the rms (root-mean-squared) error, including both amplitude and phase errors, of 0.158 m from the two-dimensional, finite-element tidal model of Lefevre et al. (2000).

The TSNOW model domain is completely confined to the Taiwan Strait (Fig. 1), in order to be consistent with a concurrent data monitoring program. Such setting, however, requires accurate description of the forcing at two open ends. Traditional practice in the three-dimensional tidal model is to specify the open-boundary forcing from results of a corresponding two-dimensional regional (larger domain) model (Davis and Furnes, 1980; Lynch and Naimie, 1993). Jan et al. (2002) followed this approach. Their three-dimensional model performance, after considerable tuning, is mixed. The tidal predictions are excellent for N_2 and O_1, good for M_2 and K_1, but disappointing for S_2 (Table 2). The rms errors for the M_2 and S_2 tides, for example, are both about 0.12 m.

Alternatively, the boundary forcing may be determined through the inverse method. Treating boundary forcing as control variables, optimal (or sub-optimal) solutions are sought through minimizing of model-data misfits. For example, Das and Lardner (1991) and Lardner (1993) used variational adjoint method in a two-dimensional tidal model of semi-enclosed sea. Ullman and Wilson (1998) and Spitz and Klink (1998) applied similar methods to the tidal estuaries. Bennett and Mcintoch (1992) and Egbert and Bennett (1996), on the other hand, used the generalized inverse method approach.

In this study, we use variational data assimilation to derive the open boundary tidal forcing. Our approach falls into the general category of four-dimensional variational assimilation schemes (4D-Var), that is, we attempt to find optimal solutions of a three-dimensional model by minimizing model-data misfits over time (tidal cycles). This approach, however, can be very expensive, as the minimization procedure involves many iterations of the three-dimensional model. To make the 4D-Var feasible in our computation environment, we adopt an incremental approach (Courtier et al., 1994). Our particular adaptation closely resembles that of Thompson et al. (2000), who used the incremental approach in the tidal model of the Gulf of St. Lawrence. Since we use the same three-dimensional model of Jan et al. (2002), our study also offers an excellent opportunity to compare 4D-Var with the traditional approach in terms of the cost and benefit.

2. Tidal sea level observations

Sea levels are obtained at 11 tide-gage stations (MT, WC, KM on small islands off mainland coast, P1, TS, HC, TC, BD, KS and P3 on Taiwan coast, and DG near Penghu Island; Fig. 1). The sea-level data are analyzed using harmonic analysis (Foreman, 1977). Table 1 lists the harmonic constants for O_1, K_1, N_2, M_2, and S_2 at each tidal station. The phase is referenced to GMT (Greenwich Mean Time). In this study, P1 and P3 on the northern and southern tips of Taiwan are treated as part of the open boundary forcing, and the remaining 9 stations are included in the variational data assimilation.

3. Model description

3.1. Three-dimensional model

The three-dimensional general circulation model is a z-level model modified from Semtner (1986) with addition of a free surface. The model is formulated under Boussinesq and hydrostatic approximations. The governing equations are

$$\frac{Du}{Dt} - fv = -\frac{1}{\rho}\frac{\partial p}{\partial x} + \nabla(A_M \nabla u) + \frac{\partial}{\partial z}\left(A_V \frac{\partial u}{\partial z}\right), \quad (1)$$

Table 1
Harmonic constants for O_1, K_1, N_2, M_2 and S_2 constituents derived from the observed sea levels at nine tidal stations

Station id	Lat. (°N)	Lon. (°E)	O_1		K_1		N_2		M_2		S_2	
			A	G	A	G	A	G	A	G	A	G
Matsu (MT)	26°10′	119°57′	0.25	88	0.31	120	0.40	42	2.10	64	0.66	96
Wuchou (WC)	24°59′	119°27′	0.25	112	0.39	147	0.35	56	2.05	89	0.55	126
Kinmen (KM)	24°24′	118°25′	0.27	124	0.33	157	0.31	91	1.70	112	0.49	152
Taipower1 (P1)	25°18′	121°36′	0.18	092	0.21	116	0.10	45	0.47	73	0.12	92
Tamsuei (TS)	25°11′	121°24′	0.18	097	0.20	126	0.20	61	0.99	80	0.30	112
Hsinchu (HC)	24°51′	120°55′	0.20	106	0.23	134	0.30	64	1.61	85	0.47	118
Taichung (TC)	24°20′	120°33′	0.20	115	0.24	145	0.33	67	1.73	90	0.50	123
Buda i(BD)	23°23′	120°09′	0.19	126	0.21	161	0.12	55	0.63	75	0.16	107
Dongee (DG)	23°15′	119°40′	0.19	125	0.20	159	0.09	53	0.50	79	0.10	112
Kaohsiung (KS)	22°37′	120°17′	0.16	129	0.18	167	0.04	333	0.18	351	0.07	353
Taipower3 (P3)	21°57′	120°45′	0.20	105	0.22	134	0.05	309	0.26	312	0.11	323

A: amplitude in m; G: phase in degrees; the reference time for phase is GMT.

$$\frac{Dv}{Dt} + fu = -\frac{1}{\rho}\frac{\partial p}{\partial y} + \nabla(A_M \nabla v) + \frac{\partial}{\partial z}\left(A_V \frac{\partial v}{\partial z}\right), \quad (2)$$

$$\frac{\partial p}{\partial z} = -\rho g, \quad (3)$$

$$\frac{\partial u}{\partial x} + \frac{\partial v}{\partial y} + \frac{\partial w}{\partial z} = 0 \quad (4)$$

in which (u, v, w) are velocity components in the (x, y, z) directions, p is the pressure, f is the Coriolis parameter, and A_M and A_V are the horizontal and vertical eddy viscosities. The y-axis is rotated 33° clockwise from the north to align with the strait axis. The model has 127×132 grids in the x and y directions with a horizontal grid resolution of 3 km. In the vertical, there are 28 layers, and the layer thickness is defined as

$$z(1) = 6.1361 \text{ m},$$

$$z(i) = z(i-1)/0.9 \; i = 2, 28, \quad (5)$$

where $z(1)$ is the top (surface) layer thickness, i is the layer index counted from the top ($i = 1$) to the bottom ($i = 28$), and $z(i)$ is the ith layer thickness. The thickness of the top layer fluctuates with sea levels.

The model basin is constructed using the NCOR 1-min high-resolution depth profile (Liu et al., 1998). The seawater density is assumed to be homogeneous. The surface boundary condition assumes no stress and the bottom boundary condition assumes quadratic drag law. Sensitivity test leads to horizontal eddy coefficient of $1000\,m^2/s$ and bottom drag coefficient of 0.0015. The vertical viscosity depends on the Richardson number following the formula of Pacanowski and Philander (1981). In the present setting of homogeneous seawater density, the vertical eddy viscosity is $0.51 \times 10^{-2}\,m^2/s$ everywhere. The model is driven by prescribed tidal sea-level oscillations on the north and south ends. The boundary conditions for currents assume zero normal gradient on open boundaries. Three different model simulations, cases A, B and C, are considered. Table 3 summarizes the essential parameters used in the three cases. In case A the tidal forcing includes (in each run) only a single tidal constituent, and in cases B and C the forcing includes all the five major tidal constituents, O_1, K_1, N_2, M_2 and S_2. Also, in case C, the bottom drag coefficient is increased from 0.0015 to 0.0025. To quantify the model-data misfit, the rms error is defined as

$$rms = \left(\frac{1}{T}\sum_{t=0}^{T}[M\,cos(\omega t - \phi) - O\cos(\omega t - \varphi)]^2\right)^{1/2},$$

where T represents a tidal cycle (case A) or 60 days (cases B and C), M and ϕ are the predicted tidal

amplitude and phase, and O and φ are the observed tidal amplitude and phase. The goodness of fit can also be evaluated using the percentage of accuracy (POA),

$$\mathrm{POA} = \left(1 - \frac{\varepsilon^2}{\eta^2}\right) 100\%$$

in which ε^2 is the error variance between observed and predicted sea levels, and η^2 is the variance of observed sea levels.

3.2. Incremental approach

The four-dimensional variational data assimilation can be regarded as an attempt to solve a minimization problem. Define the cost function

$$J(\mu) = \sum [x(t) - x_o(t)]^2, \tag{6}$$

where x_o is the observation vector, x is the corresponding model prediction, and μ is the boundary forcing. The summation is over a tidal cycle (case A) or 60 days (cases B and C). The cost function measures the model-data misfit assuming each station is weighted equally. The variational assimilation attempts to minimize J with respect to the control variables μ. The adjoint model is an efficient method in the sense that it often converges to a realistic solution regardless of the initial guess. The iteration to global minimum, however, can be very time-consuming.

The three-dimensional model may be considered as a nonlinear transformation (M), which receives μ as input and produces prediction x as output,

$$x = M(\mu). \tag{7}$$

To reduce the computation cost, Courtier et al. (1994) suggested an incremental approach. Assuming the model is weakly nonlinear, the impact of a small increment of control variable can be expressed as

$$M(\mu + \delta\mu) \cong M(\mu) + R\delta\mu, \tag{8}$$

where $R = \partial M/\partial\mu$ is the tangential linear operator of M and $\delta\mu$ is an increment from the initial guess μ. The minimization problem can be reduced to

$$J(\mu + \delta\mu) \cong \sum [R\delta\mu - (x_o - x)]^2. \tag{9}$$

Eq. (9) represents an incremental approach to 4D-Var. Given an initial guess of μ, the three-dimensional model is used to make the prediction x, and the misfit $x_o - x$ is calculated. The minimization problem of (9) is solved to find the increment $\delta\mu$. The control variable μ is then updated, and the three-dimensional model is repeated. In this approach, since only the linear model R is involved in the adjoint calculation, the computation cost is reduced compared to the solution of the original minimization problem of (6).

Use of a tangential linear model in the minimization is a step forward in terms of efficiency, especially when the original model is highly nonlinear (as in the weather forecast where the cloud physics is an important component). The possible advantage in ocean modeling is less apparent, as a three-dimensional model (albeit linear) R is used in the iteration. To simplify further, Courtier et al. (1994) suggested that it might be acceptable to replace the tangential linear model R by a simple linear model. Following their lead, we replace R by a simple linear two-dimensional shallow-water equation model:

$$\frac{\partial u}{\partial t} - fv = -g\frac{\partial \eta}{\partial x} - \alpha u, \tag{10}$$

$$\frac{\partial v}{\partial t} + fu = -g\frac{\partial \eta}{\partial y} - \alpha v, \tag{11}$$

$$\frac{\partial \eta}{\partial t} + \frac{\partial}{\partial x}(Hu) + \frac{\partial}{\partial y}(Hv) = 0, \tag{12}$$

where η is sea level, u and v are depth-averaged horizontal velocity components, H is the mean water depth, and $\alpha = 0.2$ cm/s, is a linear bottom drag coefficient. Note that the bottom stress is quadratic in the three-dimensional model but linear in the two-dimensional model. Alternatively, α can be chosen to be proportional to the bottom velocities calculated by the three-dimensional model to remove the inconsistency. We had taken this alternative approach but the results do not enhance the model performance. In this presentation, α is therefore spatially uniform to minimize unnecessary complication in our formulation of the problem. The linear model uses the identical grid layout (resolution = 3 km) and bottom topography as in the three-dimensional

model. The corresponding adjoint equations can be easily derived (e.g., Lardner, 1993). The problem of (9) is solved using the adjoint method through a standard minimization procedure (quasi-Newton method).

The control variables μ are tidal amplitudes and phases on the two open ends. There are up to 127 grid points on each open boundary. For each grid, the tidal amplitude and phase are to be determined. The total number of unknowns (~ 500) is much larger than the number of observations ($=18$). To reduce the problem size, we assume that the instantaneous tidal heights on the open boundary are piecewise linear between the two endpoints and a midpoint. The midpoint is chosen to locate approximately over the maximum water depth to take into consideration of the tidal wave diffraction over steep topography; its location was identified by a larger-scale two-dimensional model for tides in the Western Pacific (Jan et al., 2002). We further assume that the endpoints on the Taiwan coast are known, given by the tidal observations at P1 and P3. The minimization problem is reduced to 8 control variables a_i's ($i = 1, 8$), defined by

$$\eta_{sw} = a_1 \sin \omega t + a_2 \cos \omega t,$$
$$\eta_{95} = a_3 \sin \omega t + a_4 \cos \omega t$$

and

$$\eta_{nw} = a_5 \sin \omega t + a_6 \cos \omega t,$$
$$\eta_{65} = a_7 \sin \omega t + a_8 \cos \omega t,$$

where η_{sw} and η_{95} are sea levels at the west endpoint and the midpoint ($I = 95$) of the southern boundary, η_{nw} and η_{65} are sea levels at the west endpoint and the midpoint ($I = 65$) of the northern boundary.

4. Model results

4.1. Variational assimilation

We illustrate case A of model running with a single M_2 constituent. The initial guess μ is the solution of the linear two-dimensional model (10)–(12), which best-fits the observations. The rms error is 0.15 m, which is slightly inferior to the rms error of 0.12 m of Jan et al. (2002) using the two-dimensional regional model result as input. This is expected as the three-dimensional model is tuned to fit the two-dimensional regional model forcing. The misfits, $x_o - x$, are the differences between model and observations at each tidal station. The minimization problem of (9) is solved using the linear two-dimensional adjoint model, to obtain an 8×1 increment vector $\delta\mu$. The initial guess for the increment is always set to zero, and the minimization typically takes about 20 iterations. After the increment is determined, the three-dimensional model is repeated using the new boundary condition $\mu + \delta\mu$. The procedure continues until the error variance no longer decreases. Fig. 2 shows the error variance (cost function) vs. the update cycle. The incremental approach converges to the observation monotonically. The rms error is reduced from the initial guess of 0.15–0.062 m in four updates, which is a fivefold reduction in variance. The final result is much better than the rms error of 0.12 m using boundary forcing from a regional model (Table 2).

In the incremental approach the complete (three-dimensional) model is run 4 times (one for each update) and the adjoint model is iterated about 80 times. Since the linear two-dimensional model is relatively inexpensive, the total adjoint calculation of 80 iterations corresponds to about 6 times the three-dimensional model run. Thus, the

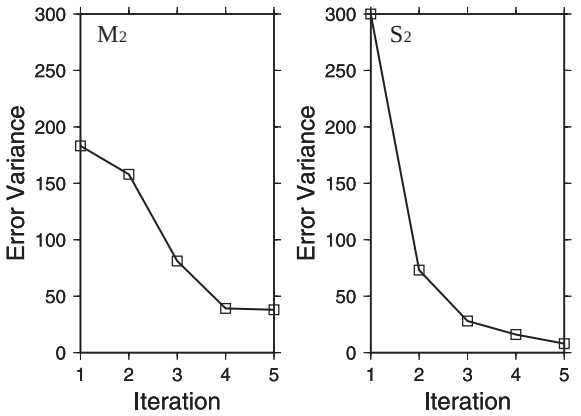

Fig. 2. The change of error variance (cm^2) with update cycle for M_2 (left) and S_2 (right) tides.

Table 2
Harmonic constants of O_1, K_1, N_2, M_2 and S_2 from the three-dimensional model with open boundary forcing derived from a regional two-dimensional model

Station id	O_1		K_1		N_2		M_2		S_2	
	A	G	A	G	A	G	A	G	A	G
	rms		rms		rms		rms		rms	
Matsu (MT)	0.24 0.008	87	0.35 0.074	137	0.39 0.8	43	1.97 0.095	63	0.66 0.186	119
Wuchou (WC)	0.27 0.024	106	0.33 0.044	150	0.36 0.061	70	1.88 0.129	87	0.66 0.118	138
Kinmen (KM)	0.28 0.028	116	0.32 0.048	145	0.27 0.028	92	1.39 0.247	106	0.48 0.014	154
Tamsuei (TS)	0.18 0.002	98	0.26 0.162	184	0.19 0.007	61	0.98 0.014	81	0.29 0.187	141
Hsinchu (HC)	0.21 0.009	108	0.34 10.8	156	0.30 0.007	66	1.61 0.020	84	57 0.145	138
Taichung (TC)	0.23 0.024	111	0.34 0.074	151	0.31 0.016	65	1.66 0.174	82	59 0.097	134
Budai (BD)	0.22 0.031	117	0.28 0.063	148	0.12 0.013	46	0.62 0.115	60	21 0.038	113
Kaohsiung (KS)	0.21 0.043	118	0.14 0.097	118	0.02 0.014	338	0.14 0.039	337	0.07 0.018	332
Dongee (DG)	0.22 0.029	117	0.28 0.061	151	0.09 0.009	58	0.45 0.059	71	0.15 0.041	126
Averaged rms	0.025		0.094		0.025		0.123		0.115	

rms: root-mean-squared error in meters.

Table 3
Summary of parameters used in the three cases. C_D is the bottom drag coefficient

Case	Driving force	Simulation time (days)	C_D
A	*Single tidal constituent*	15	0.0015
B	Five tidal constituents together	60	0.0015
C	Same as B	60	0.0025

entire minimization requires about 10 times of the three-dimensional model run, which is about the same amount of effort taken to tune a three-dimensional model.

We have applied the incremental approach to all the major diurnal and semidiurnal constituents (case A). In all cases the convergence is monotonic. Table 4 lists the final model results. The variational assimilation generally produces better results than those from using the boundary forcing from a two-dimensional regional model. We have described the M_2 tide. The S_2 tide offers an even more striking example. The initial rms error of 0.174 m is reduced to 0.028 m in 5 updates (Fig. 2). It is not clear why the three-dimensional model is extremely sensitive to the S_2 boundary forcing; though, this may help to explain why the original three-dimensional model has large error in S_2 of 0.11 m (Table 2). The POA for O_1, K_1, N_2, M_2 and

Table 4
Harmonic constants of O_1, K_1, N_2, M_2 and S_2 from the three-dimensional model with open boundary forcing derived from the incremental approach

Station id	O_1		K_1		N_2		M_2		S_2	
	A	G	A	G	A	G	A	G	A	G
	rms		rms		rms		rms		rms	
Matsu (MT)	0.25 0.003	89	0.29 0.015	121	0.39 0.007	042	2.11 0.027	63	0.65 0.011	95
Wuchou (WC)	0.29 0.028	111	0.31 0.064	140	0.36 0.066	071	1.95 0.086	91	0.57 0.016	127
Kinmen (KM)	0.38 0.078	124	0.35 0.089	136	0.29 0.018	088	1.60 0.074	113	0.46 0.027	149
Tamsuei (TS)	0.12 0.045	105	0.19 0.083	161	0.17 0.031	071	0.86 0.092	81	0.23 0.054	119
Hsinchu (HC)	0.21 0.051	126	0.29 0.071	152	0.30 0.022	070	1.55 0.072	88	0.45 0.032	123
Taichung (TC)	0.26 0.051	125	0.32 0.056	145	0.32 0.007	067	1.68 0.055	88	0.49 0.007	123
Budai (BD)	0.24 0.057	109	0.23 0.053	142	0.12 0.003	057	0.68 0.043	72	0.15 0.007	107
Kaohsiung (KS)	0.13 0.026	120	0.23 0.036	169	0.02 0.031	244	0.18 0.040	333	0.09 0.037	317
Dongee (DG)	0.23 0.035	117	0.24 0.039	149	0.09 0.026	077	0.52 0.040	85	0.10 0.022	130
Averaged rms	0.046		0.061		0.030		0.063		0.028	

rms: root-mean-squared error in meters.

S_2 in case A are 90.6%, 89.4%, 97.5%, 99.6% and 99.1%, respectively.

In a tidal model, it is common to include all major tidal constituents in a single model run. This allows consideration of nonlinear interaction between different tidal constituents. In cases B and C, we include all five tidal constituents using the boundary forcing derived from case A; the difference between cases B and C is in the bottom drag coefficient. Fig. 3 shows the spatial distribution of rms errors for the five tidal constituents. In the Taiwan Strait, the nonlinear effect is mainly through the quadratic friction. Since M_2 is the dominant tidal current, the difference between cases A and B is expected to be minor. On the other hand, POA decreases by 2–6% for N_2 and S_2, and drops to about 80% for O_1. (It is interesting that K_1 is not affected.) Increasing bottom friction (case C) improves the diurnal tide but tends to worsen the semidiurnal tide. Also, the largest errors in all tidal constituents occur at TS and WC (cf. Fig. 1). TS probably is too close to the fixed northern boundary (P1), whereas WC probably is affected by the complex local coastal geometry.

4.2. Tidal structures

Fig. 4 shows co-tidal chart and depth-averaged tidal current ellipses for the M_2 constituent

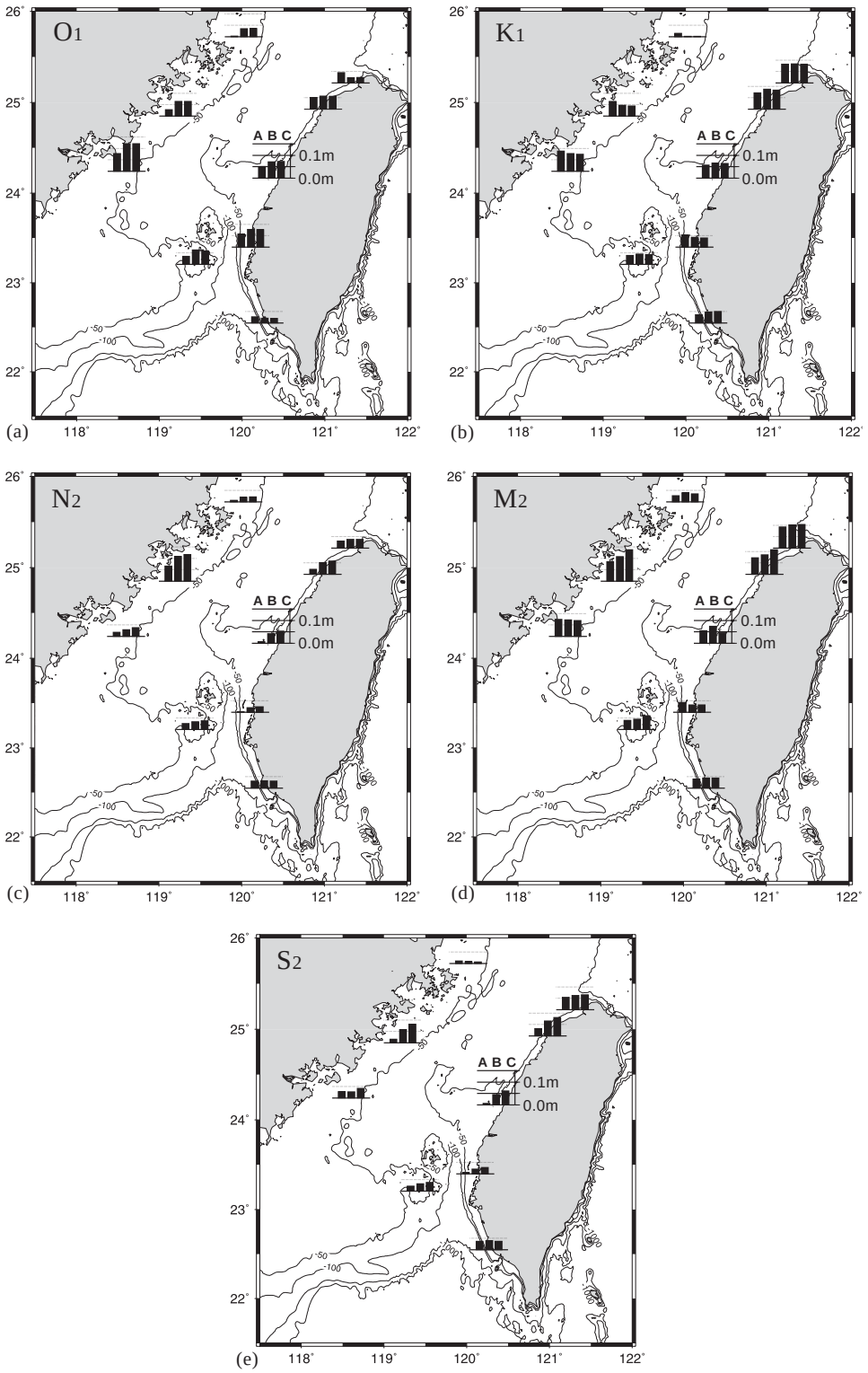

Fig. 3. Spatial distribution of the rms error of the predicted sea levels for the five tidal constituents. The error bars in each inserted frame represent rms errors of cases A, B and C from left to right.

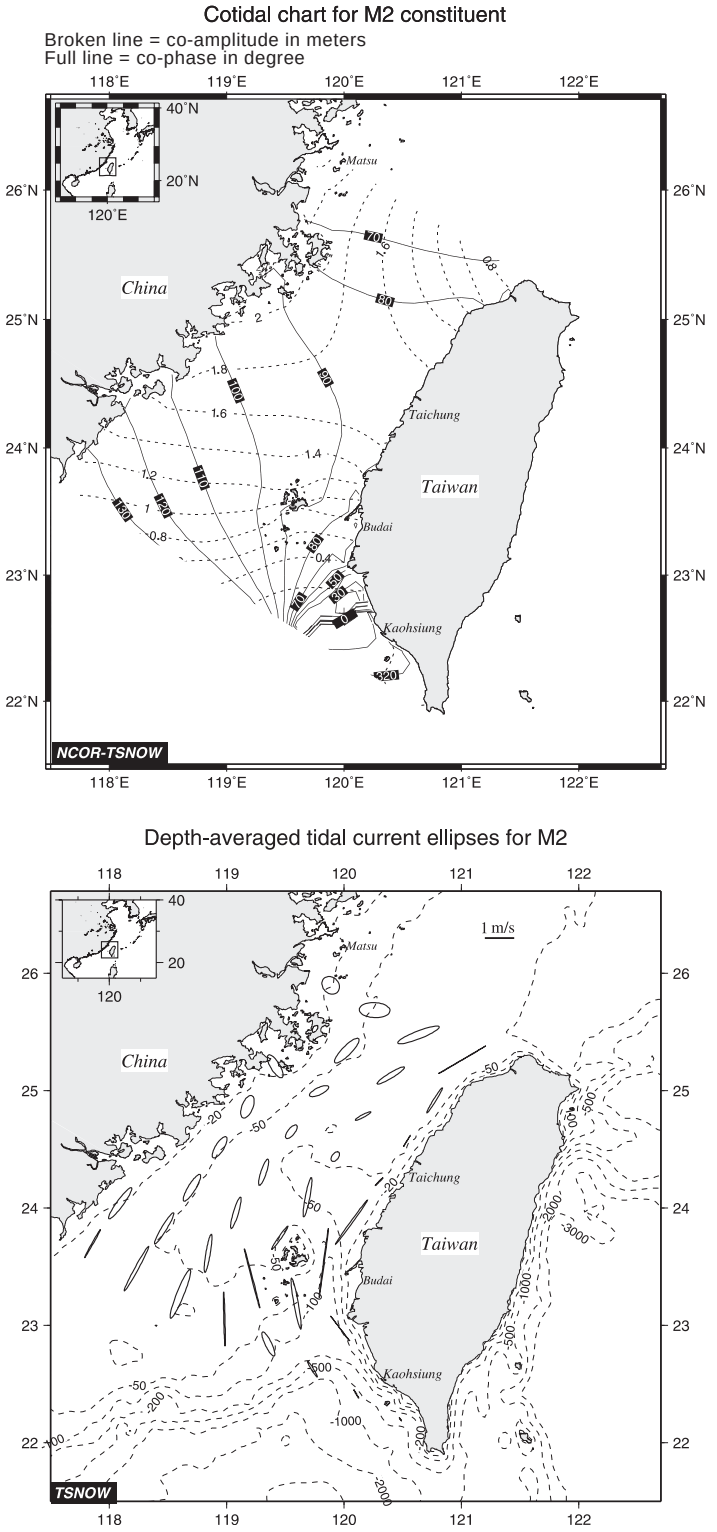

Fig. 4. Cotidal chart (upper) and tidal ellipses (lower) of M_2 tide derived from the model.

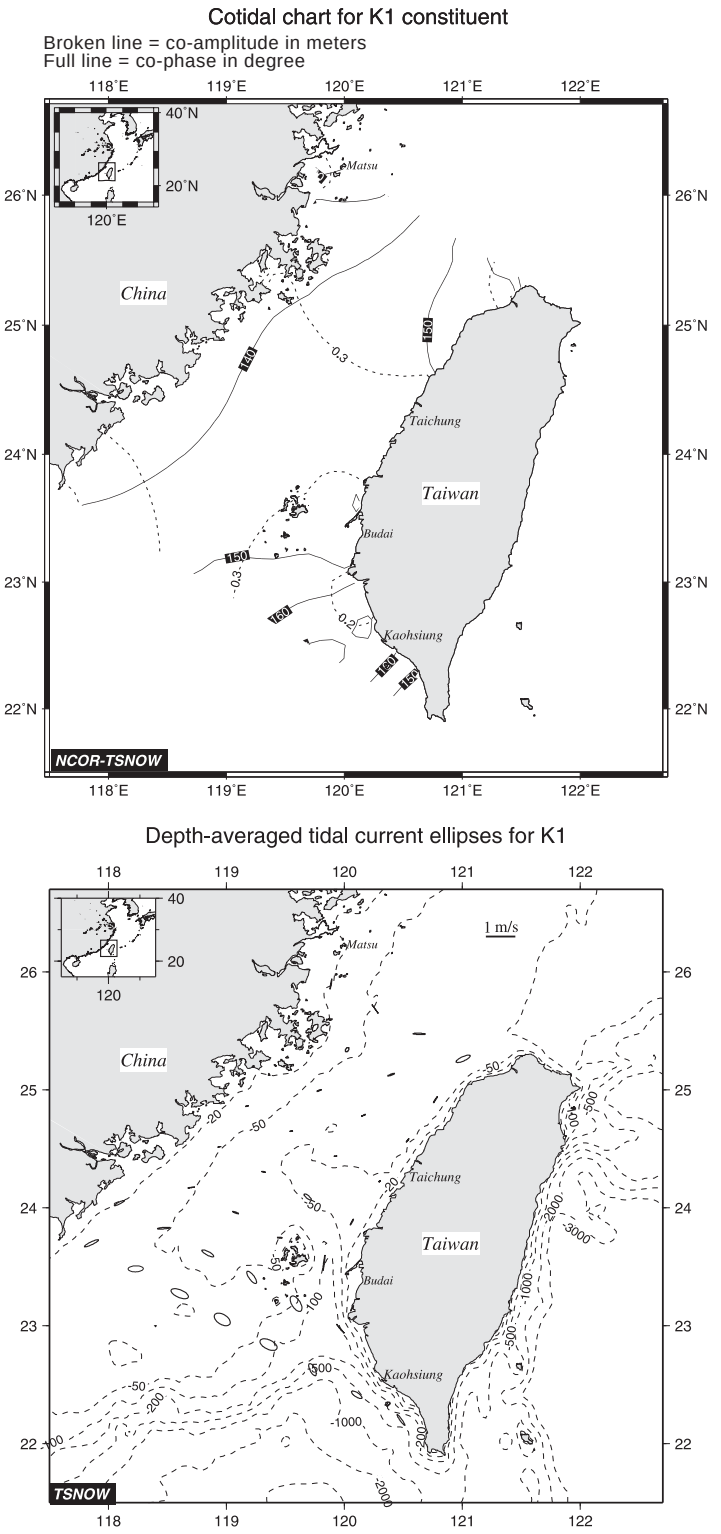

Fig. 5. Cotidal chart (upper) and tidal ellipses (lower) of K_1 tide derived from the model.

(case A). The semidiurnal tide is Kelvin wave-like along the mainland coast; the tidal wave propagates southward and its amplitude decreases offshore. On the other hand, the semidiurnal tide is a standing wave along the Taiwan coast where the tidal phase is nearly constant from HC to BD. The largest semidiurnal tidal amplitude is near WC, about 2 m. The tidal amplitude drops to about 0.5–1.5 m near the northern open boundary and to about 0.5 m over the deep (southeastern) portion of the strait. An amphidromic point near KS is indicated by small tidal amplitudes (< 0.1 m) and rapid phase progression. Tidal currents are strong over the Taiwan Banks, in the Penghu Channel, and off the northwestern Taiwan; the maximum tidal velocity is about 1 m/s. In the middle of the strait the tidal currents are weak which together with the high tidal amplitude, is indicative of an anti-node of a standing wave.

Fig. 5 shows co-tidal chart and tidal current ellipses of the diurnal K_1 tide. Unlike the M_2 tide, the K_1 tide propagates southward in the strait with little variation in amplitude. The K_1 tidal currents are mostly aligned along the strait with speeds <0.1 m/s. However, over the Taiwan Banks the tidal current ellipses tend to orient normal to the axis of the strait. The dynamics of tidal sea levels in the Taiwan Strait has been examined in Jan et al. (2002).

4.3. Model validation using ADCP data

Bottom-mounted Acoustic Doppler Current Profiler (ADCP) data from six mooring stations (WC1, WC2, WC3, WC4, EWC and PHC; Fig. 1) are used to validate the predicted tidal currents. Table 5 lists the tidal ellipse parameters for depth-averaged currents, the semi-major and semi-minor axes, orientation, and phase, for M_2 and K_1 of case A, and Table 6 lists the corresponding model predictions. Fig. 6 plots the observed and predicted tidal ellipses for the M_2 and K_1 tidal currents at the six mooring stations. For M_2, the differences in the semi-major and semi-minor axes typically are less than 0.05 m/s. PHC has the largest absolute error of about 0.1 m/s. Around PHC the water depth changes abruptly, and the consequent truncation error of local topographic feature is likely a major source of discrepancy. The relative error at PHC, though, is acceptable. WC1 has the largest relative error, which may be attributed to the poor resolution of the complex local coastal geometry. The overall rms error, which tends to exaggerate the small differences in orientation and phase, is 0.093 m/s for the M_2 tidal currents. For K_1, the differences in the semi-major and semi-minor axes are comparable to the M_2, about 0.05 m/s. This suggests that 0.05 m/s is about the threshold in tidal current prediction.

We further examine the vertical distributions of tidal currents for M_2 and K_1 at EWC and PHC for cases A and B. The vertical profiles of the semi-major and semi-minor axes, orientation and phase for the M_2 and K_1 tidal currents at EWC and PHC are shown in Figs. 7 and 8. At EWC, the semi-major and semi-minor currents are vertically uniform. The M_2 semi-major axis is slightly overestimated by 0.01 m/s (case A) and 0.02 m/s

Table 5
Tidal current harmonic constants for K_1 and M_2, derived from the observations at six ADCP stations

Station id.	Lat.(N)	Lon.(E)	K_1				M_2			
			Ma	Mi	O	G	Ma	Mi	O	G
WC1	24°59′	119°29′	0.091	0.001	29	305	0.295	0.065	31	264
WC2	24°50′	119°48′	0.047	0.017	38	238	0.221	0.105	37	252
WC3	24°39′	120°08′	0.031	0.013	31	223	0.127	0.068	32	233
WC4	24°28′	120°28′	0.015	0.000	49	213	0.053	.010	48	224
EWC	25°00′	120°08′	0.113	0.010	40	288	0.310	0.110	25	214
PHC	23°51′	119°52′	0.075	0.033	69	338	0.693	0.060	67	348

Ma: semi-major axis in m/s; Mi: semi-minor axis in m/s; O: orientation in degree; G: phase in degree; time base is GMT.

Table 6
Tidal current harmonic constants for K_1 and M_2, derived from the three-dimensional model results

Station id.	K_1				M_2			
	Ma	Mi	O	G	Ma	Mi	O	G
WC1	0.047	0.015	5	208	0.242	0.186	0	239
WC2	0.061	0.003	20	206	0.241	0.084	27	251
WC3	0.062	0.004	30	196	0.169	0.032	29	235
WC4	0.070	0.007	56	191	0.119	0.006	60	211
EWC	0.075	0.012	19	204	0.306	0.070	26	212
PHC	0.145	0.024	102	40	0.579	0.044	81	358
rms error (m/s)	0.059				0.093			

Ma: semi-major axis in m/s; Mi: semi-minor axis in m/s; O: orientation in degree; G: phase in degree; time base is GMT.

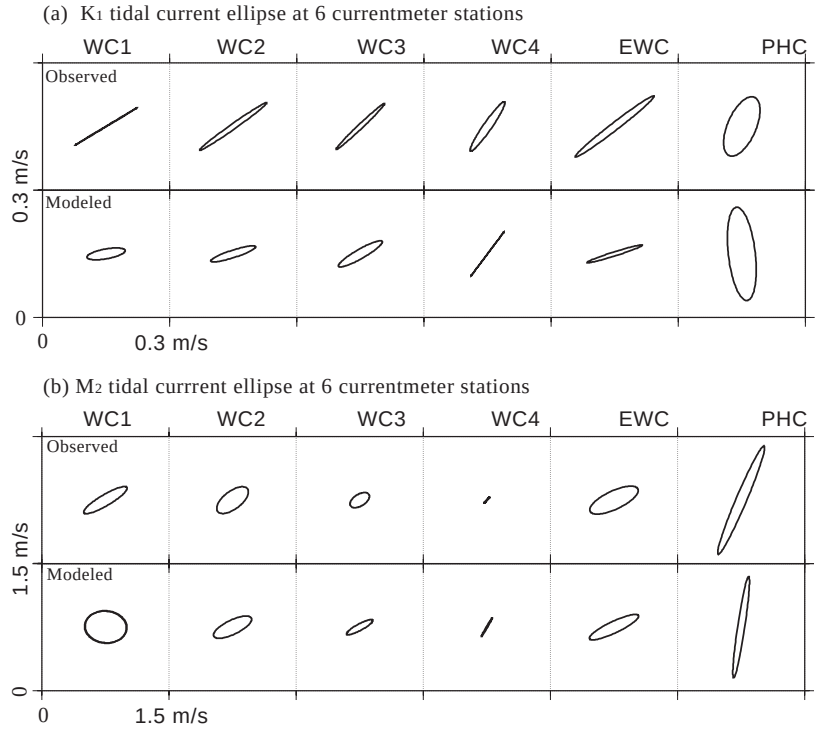

Fig. 6. Comparison of observed and predicted depth-averaged tidal current ellipses for (a) K_1 and (b) M_2 at the six bottom-mounted ADCP mooring stations.

(case B), and the M_2 semi-minor axis is underestimated by about 0.01 m/s. The orientation difference for the M_2 semi-major axis is about 3°, and the phase difference is 1°. For K_1 the semi-major axis is underestimated by 0.05 m/s and the semi-minor axis is underestimated by <0.01 m/s. On the other hand, the orientation of the semi-major axis is off by about 30° and the phase difference is about 70°. Increasing the bottom friction does not alter the predicted velocity profile (not shown). At PHC, the observed M_2 semi-major currents have distinct vertical shears in

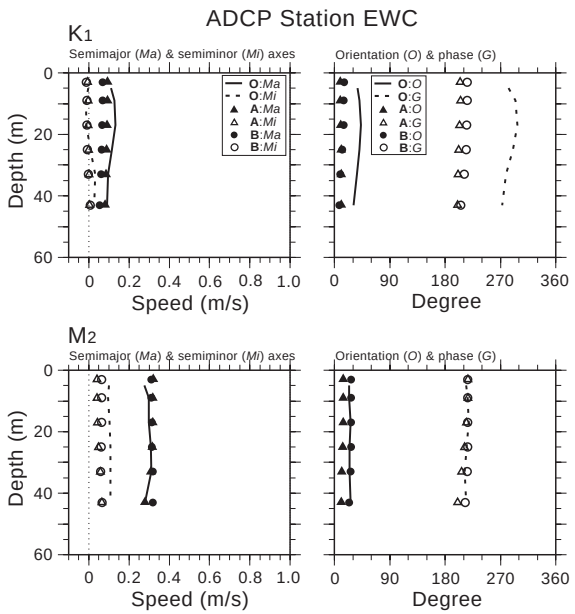

Fig. 7. Vertical distribution of the semi-major and semi-minor axes, orientation and phase of the K_1 and M_2 tidal currents at EWC. The bold character **O** represents values derived from the observations, **A** from case A, **B** from case B and **C** from case C.

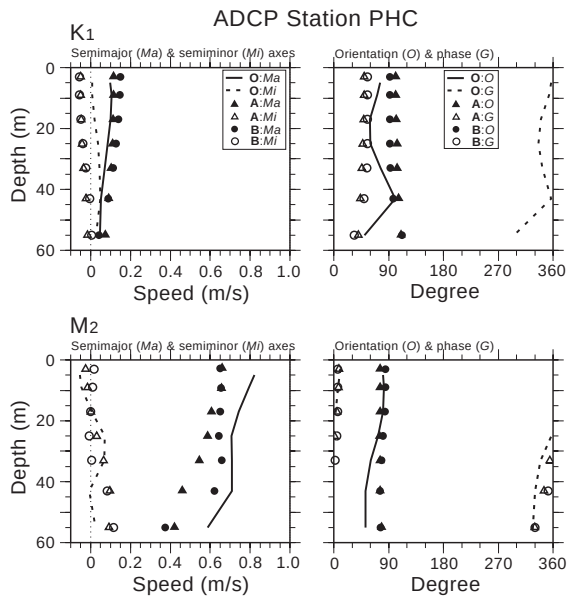

Fig. 8. Same as in Fig. 7 but for tidal currents at PHC.

the upper (<20 m) and bottom (>40 m) layers (Fig. 8). The predicted currents, however, do not indicate the observed vertical structure. The difference between model results and observations suggests the presence of a first baroclinic mode. In the Penghu Channel, the upper water column is highly stratified and the bottom slope is steep. It is likely that internal tides are generated and are phase-locked with the barotropic tide. For K_1 the semi-major axis is in good agreement with the observation for case A, but is overestimated by 0.05 m/s in the upper layer for case B. The predicted phase and orientation, however, have considerably larger difference from the observations.

5. Conclusions

The TSNOW is a complex, three-dimensional, nonlinear model system. Calibration (tuning) of three-dimensional model can be both demanding and challenging. In this study, we show that the incremental approach is both effective and efficient. The tidal sea level predictions are accurate to within few cm for all major tidal constituents. The agreement in tidal current predictions also is quite good, to well within 0.1 m/s. Our findings are consistent with Thompson et al. (2000) and Lu et al. (2001). The Gulf of St. Lawrence is a semi-enclosed basin with fairly restricted openings. The Taiwan Strait, on the other hand, is open at both ends. Success in both applications suggests that the incremental approach is applicable in most coastal seas.

In this study, the variational assimilation is limited to coastal sea level data. It would be interesting in the future to include a wider range of data in 4D-Var. In particular, it will be useful to assimilate the shipboard ADCP observations. As part of the TSNOW monitoring program, shipboard ADCP data has been routinely collected in the strait for several years. Preliminary comparisons between the shipboard ADCP analysis and the predicted depth-averaged currents show good agreement (Wang et al., 2003).

In the next stage of TSNOW, the goal is to provide nowcasting of subtidal currents. In the

Taiwan Strait, large north–south pressure gradient fluctuations had been inferred from the relationship between wind and currents (Chuang, 1985). Presumably, this pressure gradient is the result of differential adjustment of the two large ocean basins, the East and South China Seas, to the wind forcing (monsoon). The limited-area TSNOW model cannot predict the basin-scale pressure gradient. We expect to adopt the incremental approach to infer subtidal sea levels at the open boundaries.

Acknowledgements

Professors C.-S. Chern, J. Wang and T.-Y. Tang of Institute of Oceanography, National Taiwan University provided valuable suggestions for this project. T.-S. Yang, W.-H. Ho, B. Wang, S.-F. Lin and crew and technicians of Ocean Research I, II and III assisted the field work. The Central Weather Bureau kindly provided the sea-level data. This is the National Center for Ocean Research contribution number 82.

References

Bennett, A.F., McIntosh, P.C., 1992. Open ocean modeling as an inverse problem: tidal theory. Journal of Physical Oceanography 12, 1004–1018.

Chuang, W-S., 1985. Dynamics of subtidal flow in the Taiwan Strait. Journal of Oceanography Society, Japan 41, 65–72.

Courtier, P., Thepaut, J.N., Hollingsworth, A., 1994. A strategy for operational implementation of 4D-Var, using an incremental approach. Quarterly Journal of the Royal Meteorological Society 124, 1783–1807.

Das, S.K., Lardner, R.W., 1991. Variational parameter estimation for a two-dimensional numerical tidal model. International Journal of Numerical Methods Fluids 15, 313–327.

Davis, A.M., Furnes, G.K., 1980. Observed and computed M_2 tidal currents in the North Sea. Journal of Physical Oceanography 10, 237–257.

Egbert, G.D., Bennett, A.F., 1996. Data assimilation methods for ocean tides. In: Malanotte-Rizzoli, P. (Ed.), Modern Approaches to Data Assimilation in Ocean Modeling. Elsevier, Amsterdam, pp. 147–180.

Foreman, M.G.G., 1977. Manual for tidal heights analysis and prediction. Pacific Marine Science Report 77-10. Institute for Ocean Sciences, Sydney, Canada.

Lin, M.-C., Juang, W.-J., Tsay, T.-K., 2000. Application of the mild-slope equation to tidal computations in the Taiwan Strait. Journal of Oceanography 56, 625–642.

Jan, S., Chern, C.-S., Wang, J., 2002. Transition of tidal waves from the East to South China Seas over the Taiwan Strait: influence of the abrupt step in the topography. Journal of Oceanography 58, 837–850.

Kantha, L.H., 1995. Barotropic tides in the global oceans from a nonlinear tidal model assimilating altimetric tides. Part I: model description and results. Journal of Geophysical Research 100, 25283–25308.

Lardner, R.W., 1993. Optimal control of open boundary condition for a numerical tidal model. Computer Methods in Applied Mechanical Engineering 102, 367–387.

Lefevre, F., Le Provost, C., Lyard, F.H., 2000. How can we improve a global ocean tide model at a regional scale? A test on the Yellow Sea and the East China Sea. Journal of Geophysical Research 105, 8707–8725.

Liu, C.-S., Liu, S.-Y., Lallemand, S.E., Lundberg, N., Reed, D.L., 1998. Digital elevation model offshore Taiwan and its tectonic implications. Terrestrial, Atmospheric and Oceanic Sciences 9 (4), 705–738.

Lu, Y., Thompson, K.R., Wright, D.G., 2001. Tidal currents and mixing in the Gulf of St. Lawrence: an application of the incremental approach to data assimilation. Canadian Journal of Fisheries and Aquatic Sciences 58 (4), 723–735.

Lynch, D.R., Naimie, C.E., 1993. The M_2 tide and its residual on the outer banks of the Gulf of Maine. Journal of Physical Oceanography 23, 2222–2253.

Pacanowski, R.C., Philander, S.G.H., 1981. Parameterization of vertical mixing in numerical models of tropical oceans. Journal of Physical Oceanography 11, 1443–1451.

Semtner, A.J., 1986. Finite difference formulation of a world ocean model. In: O'Brien, J.J. (Ed.), Proceedings of the NATO Advanced Study Institute on Advanced Physical Oceanographic Numerical Modelling. D Reidel Publishing Co., Dordrecht, pp. 87–202.

Spitz, Y.H., Klink, J.M., 1998. Estimate of bottom and surface stress during a spring-neap tide cycle by dynamical assimilation of tide gauge observations in the Chesapeake Bay. Journal of Geophysical Research 103, 12761–12782.

Thompson, K.R., Dowd, M., Lu, Y., Smith, B., 2000. Oceanographic data assimilation and regression analysis. Environmetrics 11, 183–196.

Ullman, D.S., Wilson, R.E., 1998. Model parameter estimation from data assimilation modeling: temporal and spatial variability of the bottom drag coefficient. Journal of Geophysical Research 103, 5531–5549.

Wang, Y.-H., Jan, S., Wang, D.-P., 2003. Transport through Taiwan Strait from shipboard ADCP observations (1999–2001). Estuarine, Coastal and Shelf Science 57, 195–201.